ILASS 2008
Sep. 8-10, 2008, Como Lake, Italy

Paper ID ILASS08-12-2

PIV CHARACTERIZATION OF SPRAYS GENERATED BY CROSSFLOW INJECTION IN HIGH-DENSITY AIRFLOW

A. Bellofiore°, A. Cavaliere°, R. Ragucci*

°Dept. of Chemical Engineering, University "Federico II", Napoli, ITALY
*Istituto di Ricerche sulla Combustione, CNR, Napoli, ITALY

ABSTRACT

Determination of velocities and location of liquid droplet formed during the atomization process of a liquid jet injected in a high pressure air crossflow represents an essential step in the definition of appropriate boundary conditions for the elaboration of reliable modeling tools to be used in the design of next generation gas turbine engines exploiting such liquid atomization schemes. In this paper some exemplificative cases relative to different air-to-liquid velocity ratios and air temperatures are analyzed by means of elastic scattering imaging and particle image velocimetry (PIV). Comparison of average light scattering intensity images and velocity pattern clarify the general structure of the spray plume in the different spatial regions surrounding the liquid jet. Analysis of selected velocity components profiles better elucidate the evolution of the atomization process in dependence of the operating conditions. On the ground of the presented results a conceptual model of the liquid phase evolution could be drawn and the different physical mechanism acting in the process could be correlated to the observed phenomenology. Results presented have not only a direct applicability in any model validation activity but also help to put in correct perspective the large amount of results obtained using shadowgraphic techniques available in the literature. The conclusions represents a significant step ahead the elaboration of more physically sound and well grounded numerical models of the liquid jet atomization in cross-flow.

INTRODUCTION

Multi-hole injection is one the most interesting perspectives for improving the control of combustion processes in gas turbine and in furnaces. The success of such strategy is based both on a better controlling of the atomization process of liquid jets in cross flow condition [1, 2] and, in turns, on better understanding of the evolution of such type of process. Unfortunately due to the complexity of the process which sums the complexities related to the atomization structure of both liquid jet (gas velocity parallel to the liquid interface) and drop-like structures (gas velocity parallel to curvature) there is not yet available any comprehensive model of all the atomization parameters. Nevertheless, a quite complete characterization of bent profile of ensemble averaged shadowgraph of the jet in terms of semi-empirical interpolating correlations is available in a broad range of the external parameters [3-6]. Among these the model presented in [6] is able to give a realistic representation of the upstream profile of the liquid jet in a spatial domain that is limited along the curvilinear profile by the break-down position, where the coherence of the liquid jet is lost. Such position can be either predicted in a satisfactory approximation by means of a semi-empirical correlation or can be obtained in a more accurate approximation by means of a relatively simple statistical elaboration of the shadowgraphies [7].

These achievements allowed giving better boundary conditions prescriptions to single phase fluid-dynamic models in identifying the spatial loci from where the liquid phase can be thought to be injected in forms of blobs or droplets, of which size and velocity are usually assigned on the ground of hypothetical assumptions. In other words a lack of models and/or semiempirical correlations characterize the state of art in this part of the atomization field (velocity and size of droplets), which is mainly due to the scarce literature on the experimental characterization of such quantities in this configuration [8, 9].

This paper contributes to enrich the experimental data base on which "more" detailed and physically grounded models can be developed by producing an as much as possible accurate statistical description of the jet by exploiting both Mie scattering and 2D-PIV techniques. Validity of the results is also discussed in relation to those obtained by means of shadowgraphic techniques [6, 7].

EXPERIMENTAL SET-UP AND PROCEDURES

Details of the experimental facility have been presented elsewhere [6,7]. Due to lack of room are here only reported the main features relevant to the presented results. The experimental facility is designed to reproduce geometry and working conditions comparable to the operation of the premixing channel of a LPP gas turbine, the maximum airflow pressure and temperature being 4 MPa and 700 K, respectively. The test section is a straight channel with rectangular 25x25 mm cross-section. The injector is a plain nozzle with 0.3 mm outlet diameter (D). A 45° taper introduces the liquid flow to the terminal straight section of the nozzle having a length-to-diameter aspect ratio equal to 4. A Pitot tube, placed about 280 mm upstream the injection point, was used to monitor the air velocity in the channel midpoint during the tests. Liquid and gas velocities maximum error was estimated to be lower than 5%.

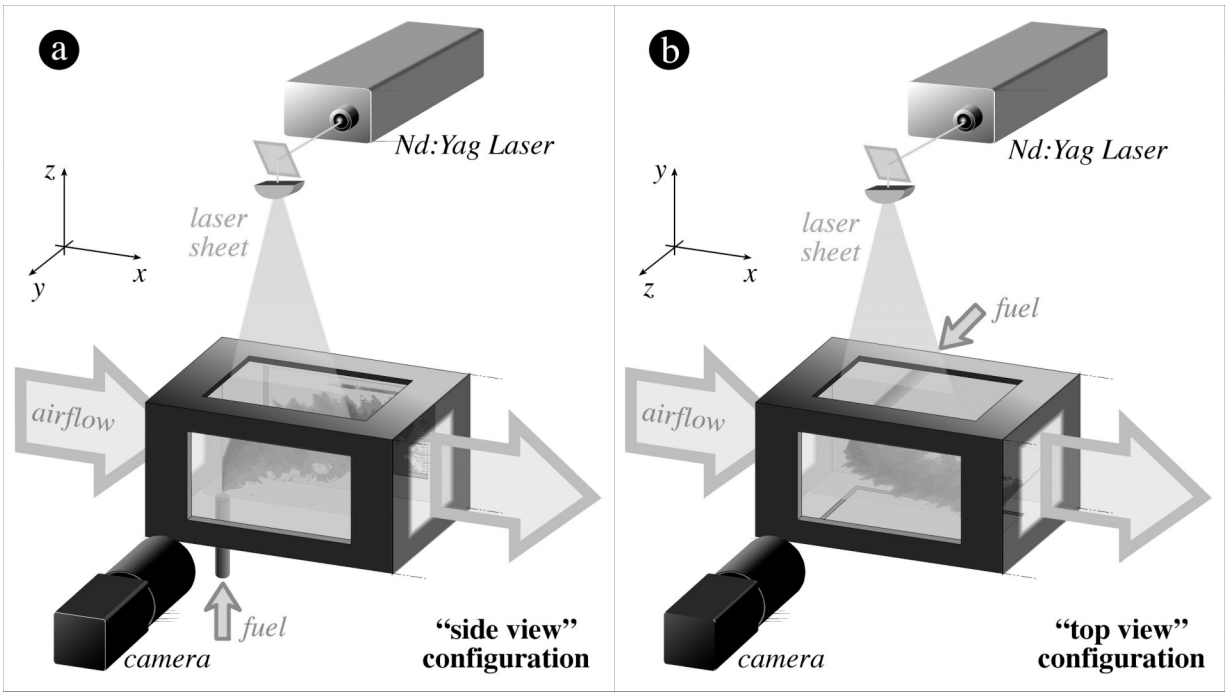

Fig. 1 Sketch of the diagnostic setup, in either side (a) or top (b) configuration.

A 2D-PIV equipment by TSI, composed of a Nd:YAG double pulse laser, a 4 Megapixel 16-bit digital camera and a synchronizer, was used. Two laser pulses in a short time interval are shot and the Mie scattering signal is detected by the camera at a 90° angle. The system has been used in two configurations. The former, sketched in figure 2a, is referred to as "side view". The plane of the laser sheet coincides with the plane individuated by the gas main flow and liquid injection axes, named x and z, respectively. All the measurements reported here were collected in the plane $y = 0$, which is the plane intercepting the nozzle axis. The latter configuration (figure 2b), referred to as "top view", requires the illumination plane to be aligned with the axes x and y.

Key parameters for the PIV are the spatial resolution of the image and the time delay between illumination pulses.

A resolution of 12 μm per pixel was chosen to trade off between measurements resolution and statistical significance of the image ensembles. This resolution, for a 4 Megapixel camera, results in a field of view nearly equal to the width of the test channel. This setup was adopted for side view measurements. In consideration of the characteristic velocities of the two phases a time delay of 4 μs was selected. The top view measurements were performed using a resolution of 4 μm per pixel and a time delay of 2 μs. The image processing by TSI Insight™ software was performed by selecting "NyquistGrid" as the grid engine and "HartCorrelator" as the correlation engine. The interrogation region was set to 64x64 pixels, with maximum accepted displacement equal to 32 pixels. Minimal validations criteria were set up, aiming to reject velocity magnitudes significantly higher than reference injection velocities.

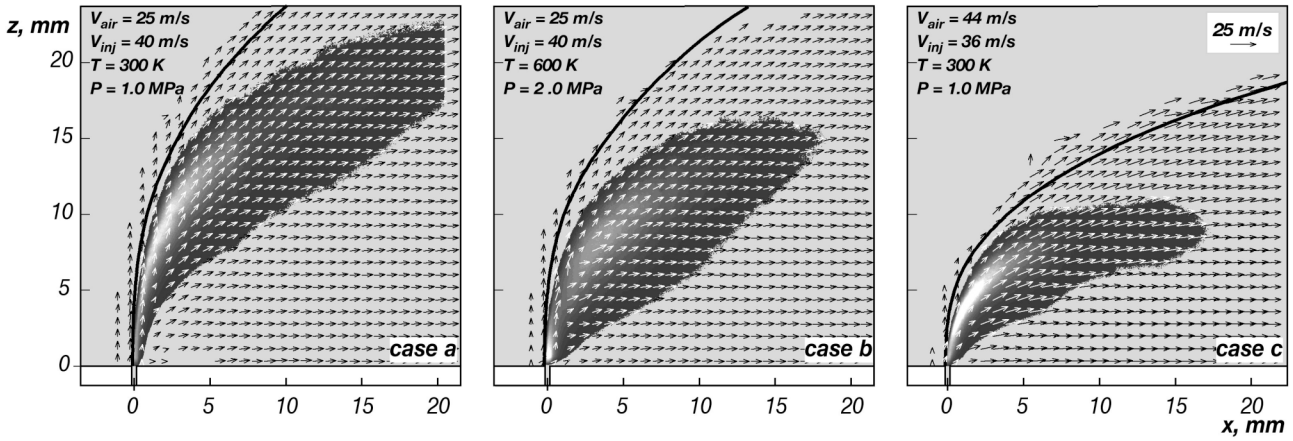

Fig. 2 Comparison of the Averaged Mie scattering images and of the velocity magnitude vectorial fields measured in the side-view configuration. Profiles are those obtained by using the correlation proposed by Ragucci et al, 2007.

The evaluation of the velocity proceeds from the values of spatial displacement and time shift. As regards the time shift, the overall inaccuracy of the PIV system was declared to be well below 1%. As regards the evaluation of the displacement, the main source of inaccuracy is the spatial calibration procedure and was estimated to be in the order of 1%. Therefore the maximum error connected to the diagnostic system is small if compared with the accuracy resulting from the experimental setup [6].

RESULTS

In this paper a set of 3 experimental conditions has been investigated. The reference condition (case a) features kerosene injected, through a 0.3 mm plain nozzle, at 40 m/s initial velocity into an air crossflow at 300 K temperature, 1.0 MPa pressure and 25 m/s undisturbed mean velocity. The second condition (case b) differs from the reference case as regards air temperature and pressure, which are 600 K and 2.0 MPa, respectively. Finally the third condition (case c) holds pressure and temperature of the baseline condition, but air and liquid velocity are modified to 44 and 36 m/s, respectively. It should be stressed that the air density was kept at the same value for all the conditions here investigated. Moreover cases a and b share the same liquid-to-air momentum ratio q (about 170), which is instead lower for the case c (45).

The overall behavior of the three sprays under investigation are summarized in Fig. 2, which basically reports images of the Mie scattering signal averaged over samples of 500 (cases a and c) and 250 (case b) frames.

Figure 2 also features vector maps of the average velocity detected by the PIV system. Finally the black continuous lines in Fig. 2 represents an estimation of the spray penetration profile, as predicted by the empirical model proposed in [6] and developed on the basis of statistical analysis of spray images collected by means of a flash shadowgraph diagnostic setup.

It is obvious in Fig. 2 that the area of the spray, as results from the average Mie scattering images, is significantly smaller than the area covered by the vector maps. This difference is due to the fact that in the average images the pixels with scattering intensity lower than 5% of the highest detected intensity were discarded to make the images more “readable”. This blanking is operated on averaged images, whereas the vector maps are:

(1) evaluated over pairs of images, far less homogeneous than average ones, characterized by the presence of zones with no signal (giving no or low contribution to average images) and zones where an intense signal allowed for velocity evaluation;

(2) averaged, for each interrogation region, not on the number N of sampled images, but on the number $n(i,j)$ of images where a vector has been detected in the region (i,j).

For all the investigated conditions the velocity maps share some common features. Vectors placed in the zone comprehensive of upper boundary and highest scattering intensity show that here the droplets initially follow the direction of liquid injection and are later bent by the air drag. The upper boundary of the velocity maps closely resembles the behavior predicted by the empirical penetration model, and moreover the velocity vectors appear to be tangent to the predicted penetration. On the other hand in the whole leeward zone of the spray velocity vectors appear to be mostly aligned with the airflow direction. As regards the velocity magnitude, in cases *a* and *b* it shows a zone of maximum values close to the region of highest scattering intensity. In this zone velocity magnitudes are coarsely between air and liquid velocity. In the vicinity of the upper boundary and in the leeward zone velocity magnitudes are much closer to the air reference velocity. Different is the situation of case *c*, where velocity magnitudes are smaller near the injection point, where they are similar to the liquid injection velocity, while the spray progressively accelerates along the x direction and almost reaches the air velocity.

It is interesting to point out that the zone of highest velocity and scattering intensity is located more downstream than the leading edge of the vector map, thus indicating the presence of droplets detached from the liquid jet and entrained by air in the upstream region of the spray.

Figure 3 presents quantitative results about the orientation of the velocity vectors and the z-component of velocity, for cases *a* (left) and *c* (right). In the lower part of the figure, the spray area is represented by a contour plot of the angle of the velocity vectors with respect to the x axis. The contour plot is overlapped to a grey silhouette resulting from the binarization of the average scattering image using a threshold at 50% of the maximum value. In the upstream zone, close to the injection point the droplets are nearly parallel to the liquid injection velocity for either condition. The contour lines clearly show the progressive bending of the spray. Condition *c*, in particular, presents steeper gradients of the spray orientation, due to the stronger air momentum. On the downstream side of the spray the contour lines are coarsely parallel to the leeward profile of the grey silhouette, supporting the idea that the silhouette could be considered a representation of the denser liquid core.

On the top of Fig. 3 profiles of the z-component of the detected velocities are plotted as a function of x and for selected values of z. At least for the lowest values of z, the profile presents a maximum of velocity, plotted as empty circles, which shifts downstream and decreases in value as z increases. At the highest values of z the z-velocity profiles lose the maximum and appear uniformly decreasing as x increases. At the beginning of the spray the highest detected velocities are in prevalence directed in the z-direction. In addition, in the case *a* the highest velocities are even higher than gas reference velocity. Therefore these velocity peaks hold the momentum of the liquid jet, representing evidence of its placement. It must be underscored that the z-components of the detected velocities never reach the liquid injection velocity, even at the lowest values of z, indicating that the air drag rapidly decelerates the droplets detached from the liquid jet. The locations of the maxima of z-velocity are reported in the bottom part of Fig. 3, as full circles. It is obvious that the peaks fall into the silhouette for every case where a maximum is detectable. This further supports the idea that the zone of highest scattering intensity is strongly related to the location of the most coherent zone of the spray.

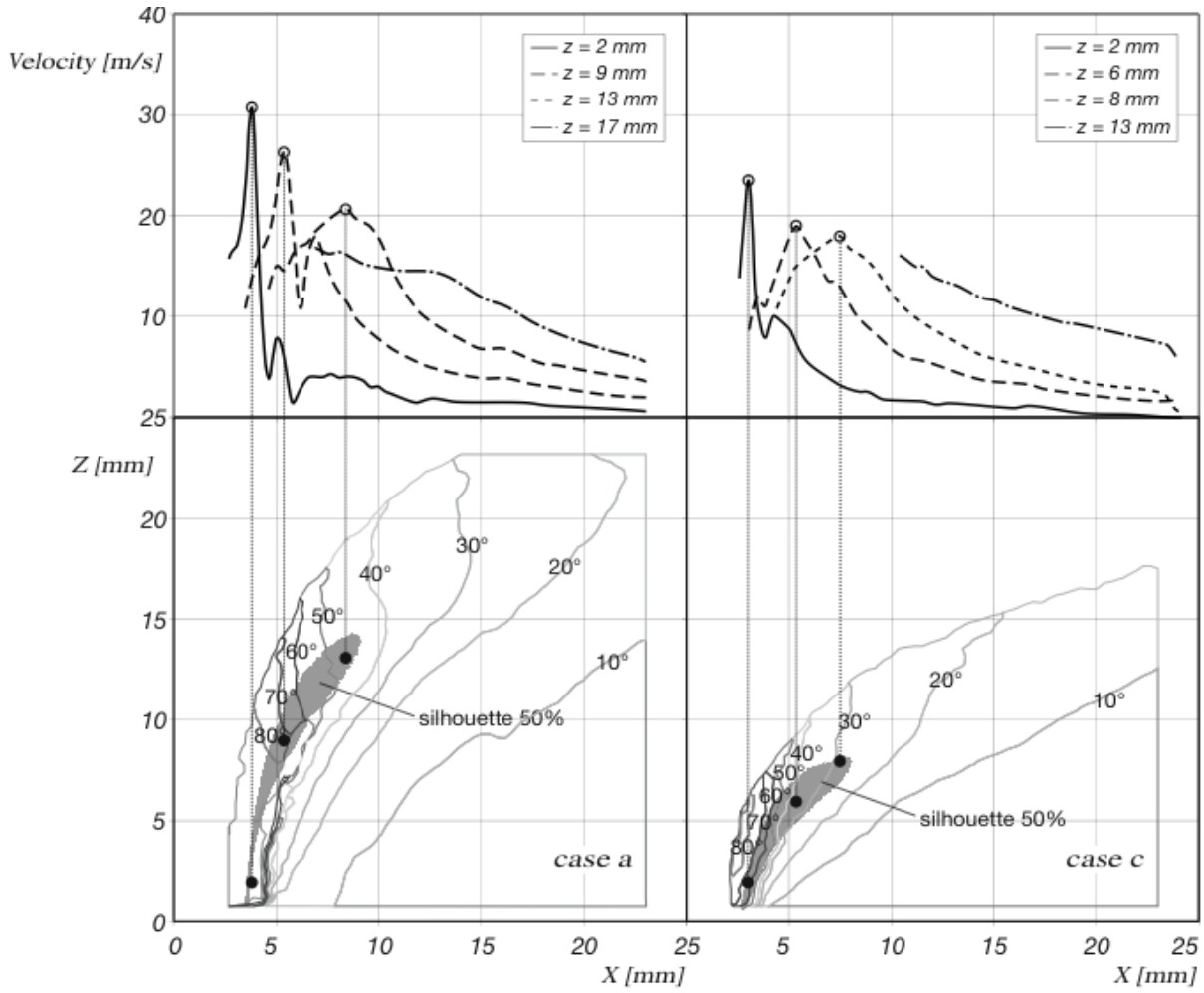

Fig. 3 Velocity field orientation with respect to the nozzle axis and selected velocity profiles at fixed z-values for the cases a and c.

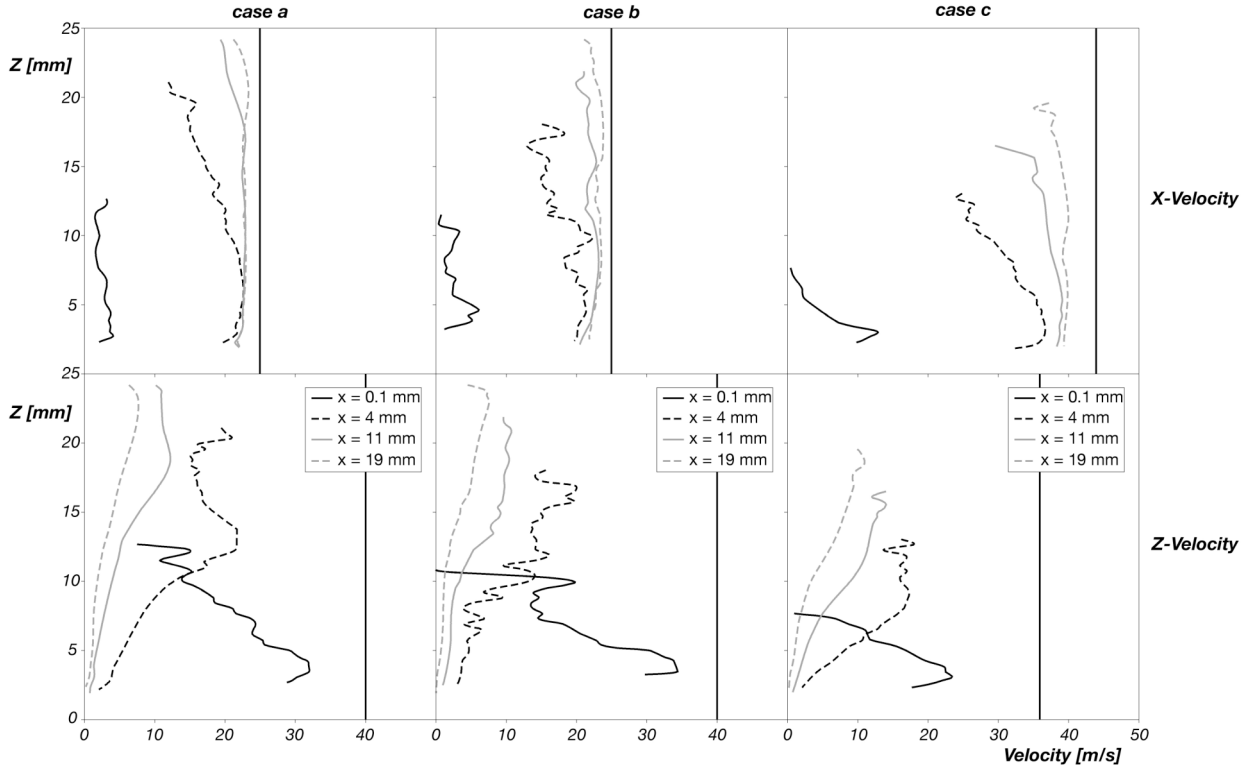

Fig. 4 Vertical (along z) profiles of x and z components of velocity at selected x positions for the cases a, b and c.

Figure 4 presents profiles of x-component (upper row) and z-component (lower row) plotted as a function of the coordinate z and for selected values of x. The profiles have been evaluated for case *a*, *b* and *c* (right, middle and left row, respectively). The plots have the coordinate z on the vertical axis in order to keep them comparable to previous plots. As regards the x-velocity, for all cases it is observed that it is very small close to the injection point (x=0.1 mm) and it rapidly increases up to a value comparable with the reference gas velocity. At the second selected step (x=4 mm) the detected x-velocities are already about 80% of the gas velocity, indicated with a continuous vertical straight-line. It is to be noted that, especially for the higher gas velocity case *c*, the droplets generated in the earlier stages of the atomization process (i.e. at lower z) speed up faster than the droplets in the top part of the spray. This fact could be explained as follows: as suggested by the observation of Fig. 2, droplet generation by stripping mechanisms (mostly effective at the beginning of the jet) occurs along a curved profile, supposedly represented by the silhouette of the spray core. This means that at a certain x value the droplets in the lower part of the spray have had more time to be accelerated by the air drag, thus resulting in higher velocity. At the latest x station (x=19 mm) the spray velocity is close to the reference gas velocity and uniformly distributed along the z direction. The higher slip detected for case *c* (about 10% of gas velocity) is attributable to the shorter time available for drop acceleration, due to the higher gas velocity.

The z-component of detected velocities is reported in the lower row of Fig. 4 as a function of z. Liquid injection velocities are also reported as a continuous vertical straight-line. It is evident that at the beginning of the spray (x=0.1 mm) z-velocity is the main contribution to the overall velocity. The closer to the injection point the faster the droplets are due to their deflection by the airflow. This behavior is common to all the z-velocity profiles at x=0.1 mm. Situation is completely different at later x stations, where the distribution is still non-uniform, but the highest values lay on the top part of the spray, for all the three cases under investigation. This could be attributed to the fact that the droplets intercepted at higher x positions are either:

stripped and allegedly smaller than those at lower z, therefore rapidly aligned with the airflow;

droplets resulting from the liquid jet collapse at higher z, whose size is more broadly distributed, so that with higher inertia they can longer retain the momentum of the liquid jet.

The total velocity profiles, resulting from the composition of the two velocities components, are not reported due to lack of room but some relevant features deserves some comments. In the cases *a* and *b*, where air velocity is lower and droplets have more time before leaving the investigated area, the total velocity profiles at x=4 mm are nearly overlapped to the profiles at x=19 mm, thus indicating that the spray quickly reaches its terminal velocity. This fast decrease of the slip velocity between gas and liquid is to be considered in the evaluation of the effectiveness of the atomization process. In case *a* a cloud of droplets with residual larger velocity survives even at the highest x values. This velocity peak gradually reduces and shifts toward higher z positions, thus providing further evidence that these droplets are the leftovers of the collapsed jet. In hot airflow as well as in the higher gas velocity cases the velocity peak was not observed. These cases share a gas Weber number (320 and 480, respectively) higher than case *a* (100), and this fact suggests that the velocity peak can be wiped off by more intense atomization levels. This compare to the shorter, less narrow and intense scattering image observed in case *b* (see Fig. 2) with respect to case *a*. This difference, in view of the same q value of the two cases, has to be attributed to the higher Weber number implied by a lower surface tension value at higher temperature.

Experimental data collected in "top view" configuration are presented in Fig. 5 only for the reference case *a* due to lack of room but there is no or little difference in the considered cases. In particular Fig. 5 shows the velocity vector maps obtained at three different heights above the injector, x=4, 8 and 12 mm. The vector maps are overlapped to the averaged Mie scattering images. At the lowest height (x=4 mm) the placement of the detected droplets assumes a bow shape. This effect seems to be attributable not only to obscuration of the inner droplets due to the interposition of dense spray between the illuminated droplets and the camera, but it also indicates a real lack of droplets in the near wake of the liquid jet at low z values.

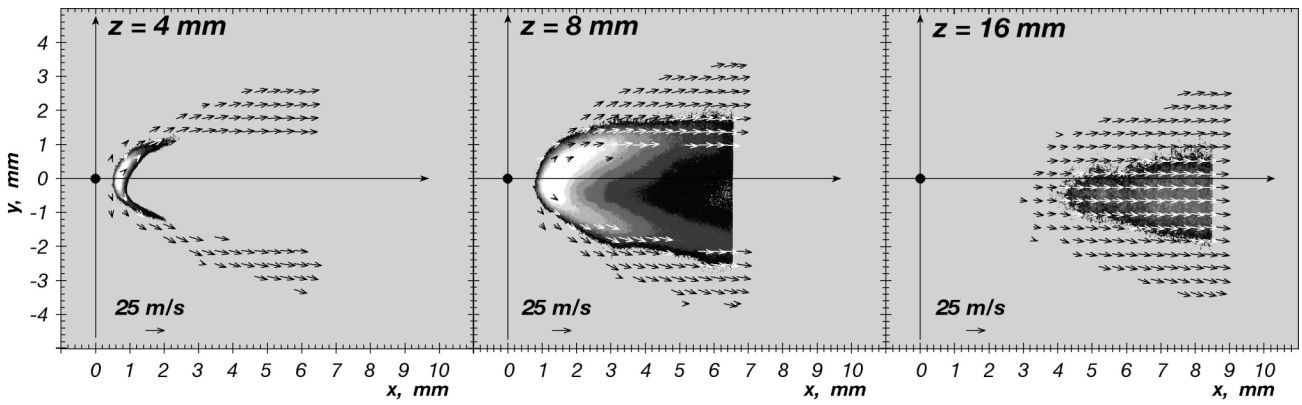

Fig. 5 Comparison of the averaged Mie scattering images and of the velocity magnitude vectorial fields measured in the top-view at selected z positions for case a.

As matter of fact the "side view" of the case *a*, reported in figure 2, clearly shows that at y=0 mm the signal is really poor at low heights. Data collected in "side view" at *y*=2 mm (not reported in this paper for lack of room) show a much stronger signal in the same zone. As a consequence it can be stated that, at the beginning of the spray, atomization occurs by means of stripping mechanisms effective on the sharpest edges of the deformed jet cross-section. The droplets detached in proximity of the windward boundary of the liquid jet show trajectories that seem to follow the path of the airflow around the obstacle represented by the liquid jet. Further downstream droplets still hold a residual velocity component in the y direction. At *x*=8 mm and *x*=16 mm the scattering signal is stronger even in the central zone of the spray, although at the intermediate height the obscuration effect prevents velocity evaluation. As far as a coherent liquid structure survives, the scattering signals shows bow shaped gray levels and velocities exhibit the behavior described for the map at *x*=4 mm. At the highest height the droplets are all coarsely aligned with the airflow.

DISCUSSION AND CONCLUSIONS

The most striking features evidenced in the presentation of the results are related to three main zones, which are conventionally named upstream, central and downstream in relation to their position along the gaseous stream in respect to the liquid jet core.

1) Upstream region, in which:

The upstream contours of the PIV images are nearly coincident with the upstream profiles obtained by the shadowgraphies, which are here reported as the predicted leading edges (solid lines in Fig. 2), therefore they bound the real periphery of the spray, where the scattering intensity is so low that cannot be detected over the noise level;

The velocity directions along the upstream contours of the PIV images nearly parallel the leading edges;

The velocity intensities along the upstream profiles increase along the curvilinear upstream profiles reaching an asymptotic value.

The first observation allows retrieving the massive amount of data that have been collected in the past both in this and other groups by means of shadowgraphic techniques. Therefore all the data and their interpretations still represent a corpus of knowledge consistent with the images presented in the previous section.

The last two points infer that, independently on the spray structure, characteristics of velocity intensity and direction are relative to gaseous fluid-dynamics in the interaction between unperturbed gas pattern and the liquid jet obstacle. The peripheral part of the spray undergoes a continuous bending and, above all, accelerates continuously up to the location where the velocity intensity does not change any longer. These are the same features that characterize an impinging jet along and near a solid surface with the only difference that in the case of the liquid jet the obstacle interface is moving along a curvilinear coordinate in patches, blobs and fragments.

2) Central region:

The scattering intensity in the vertical plane is not bounded by upstream contours of the PIV images and it is bent more and more far from the nozzle in respect to the leading edge;

The velocity direction in the cross section planes parallels the scattering intensities contours (see Fig. 5);

The horizontal velocity components (see Fig. 4) reach a constant value in the near field of the spray before z=8 mm (i.e. $z/D = 27$), whereas the vertical components decrease for all the explored conditions at least up to z=25 mm (i.e. $z/D = 83$);

The velocity and scattering intensity patterns do not change significantly up to 600 K and 20 bar, provided that the comparison is done with the same q value;

As general comments to all these points it is relevant to underline that the central part of the liquid jet can be thought as a curvilinear cone whose axis is the loci of liquid blobs or droplet which accelerate or decelerate up to the velocity intensity of the gaseous flow. The directions of these velocities are always tangent to the scattering intensity iso-lines.

This statement is relevant, because it can represent the first possibility to assign the average liquid velocity of the liquid spray on the ground of measured quantities depicted in a simple conceptual scheme

3) Downstream region

There is a well defined area of low velocity intensity downstream of the liquid jet in the near field region.

This region can be considered the zone where wake patterns develop and large vortical structures like horse –shoe vortices develop. Therefore the velocity averages are weighed on values, which can be also negative and representative of fluctuation phenomena.

ACKNOWLEDGEMENT

This work has been partly supported by the European Community in the framework of the TLC contract, Contract N°AST4-CT-2005-012326. Authors thank A. Picarelli and V. D'Antuono for their contribution to the experimental work.

REFERENCES

1 K. Bunce, J.G. Lee, D.A. Santavicca, 44th ASME Conference, AIAA, Reno, USA, 2006, paper ID 1225.

2 P.K. Wu, K.A. Kirkendall, R.P. Fuller, J. Prop. Power 14 (2) (1998) 173-182.

3 B.J. Masuda and V.G. McDonell, 10th ICLASS Conference, ILASS-Asia, Kyoto, Japan, 2006, paper ID 275.

4 J. Becker and C. Hassa, Atom. Sprays 11 (1-3) (2002) 49-67.

5 J.N. Stenzler, J.G. Lee, D.A. Santavicca, W. Lee, Atom. Sprays 16 (8) 887-906.

6 R. Ragucci, A. Bellofiore, A. Cavaliere, Proc. Comb. Inst. 31 (2007) 2231-2238.

7 R. Ragucci, A. Bellofiore, A. Cavaliere, Atom. Sprays 17 (1) (2007) 47-70.

8 E. Lubarsky, Y. Gopala, O. Bibik, B.T. Zinn, 44th ASME Conference, AIAA, Reno, USA, 2006, paper ID 1342.

9 O.M. Elshamy, Experimental Investigation of Steady and Dynamic Behavior of Transverse Liquid Jets, PhD Thesis, University of Cincinnati, USA, 2006.